Viscoelastic and Electrical Properties of Self-Assembled Monolayers on Au(111) Films

M. Salmeron,* G. Neubauer,† A. Folch,‡ M. Tomitori,§ D. F. Ogletree, and P. Sautet‖

Materials Science Division, Center for Advanced Materials, Lawrence Berkeley Laboratory, University of California, Berkeley, California 94720

Received May 21, 1993. In Final Form: September 14, 1993•

The interaction between Pt-13% Rh tips (of ~1000 Å radius) and (111) oriented gold films covered with alkanethiolate monolayers has been studied with an atomic force microscope (AFM) of the interferometer type. The thiol molecules, with structural formula H-S-$(CH_2)_n$-CH_3 had 12 and 22 carbon atom chains (n = 11 and 21). The cantilever of the AFM was forced to oscillate near its resonance frequency while the amplitude and phase of the oscillation at the free end supporting the tip were measured. These two parameters changed rapidly when the tip approached within a few nanometers of the surface. This allows us to investigate the viscoelastic properties of the surface films. We found that the thiolate layers respond to the applied load in a reversible way. Upon contact with the layer, the tip oscillation amplitude decreased to 10-20% of its original value and remained at this level until the load reached (7 to 15) × 10^{-6} N. At loads below 1 × 10^{-6} N, the tip-sample interaction is mainly elastic and no visible marks can be seen in the ac-AFM (attractive mode) images. Above that value, the gold substrate was found to yield plastically. This plastic threshold was identical to that found in bare gold. With an applied bias, tunnel current was found upon initial contact of the tip with the alkyl chain. This current is very sensitive to defects of the layer and to the compressive force applied by the tip. A theoretical calculation was performed to explain the effects of the adsorbed organic molecules on tunnel currents.

1. Introduction

An understanding of the microscopic phenomena that control adhesion, friction, and lubrication can be obtained by performing experiments where the contacting bodies have well-defined geometries and composition and where the applied forces are small enough that atomic scale phenomena are dominant. Two instruments have been developed to approach these ideal conditions. One is the surface force apparatus (SFA) developed by Israelachvili.[1] In this device the contact occurs over an area several micrometers in diameter. The other is the atomic force microscope (AFM) developed by Binnig et al.[2] The sharp tip of the AFM is a convenient model of a single asperity. In addition the AFM can be used to image the surface in the weak repulsive or in the attractive modes so that little or no perturbation is introduced by the imaging process itself. Both instruments allow the accurate measurement of the forces applied in the normal or horizontal directions to the surface. Not surprisingly an increasing number of papers have appeared recently where AFM is used to image and to investigate the mechanical properties of surfaces with organic layers and lubricants.[3-5]

The present paper is a continuation of work presented recently[6] where AFM was applied to study the mechanical properties of bare gold thin films of (111) orientation grown on mica and on silicon wafers. In the present work we use self-assembled monolayers of alkanethiolates on the same gold substrates as models of lubricant films. The formation, structure, and properties of these films have received considerable attention in recent years.[7] They are known to form compact and well-ordered structures[8-10] often with a $\sqrt{3}\times\sqrt{3}R30°$ periodicity relative to the gold substrate. Space filling is achieved by tilting the molecular axis[11] by 20-30°.

As we will see, the strong metallic adhesion between the tip and the substrate observed on bare gold is drastically modified by the presence of the alkanethiolate monolayers. However, the plastic behavior of the substrate is not altered by the presence of these organic monolayers. We have also investigated the conductivity of the films by measuring the current flowing between tip and surface as a function of bias voltage and applied force. We will see that under large applied forces the surface is disrupted noticeably at the edges of the contact zone where the gold substrate has been sheared during the plastic deformation. Of special interest is the possibility offered by the AFM technique to study the elastic and viscous properties of monolayers when in contact with a vibrating tip.[12] We will show that when the lever supporting the tip is driven to oscillate near its mechanical resonance frequency, the amplitude and phase of the oscillation are sensitive probes of the viscoelastic properties of the films.

2. Experimental Section

2.1. Microscope Head and Tips. The experiments were conducted with an AFM that uses interferometry to measure the

† Present address: Intel Corporation, 2200 Mission College Blvd, Santa Clara, CA 95052.

‡ Departament de Física, Universitat de Barcelona, Spain.

§ Department of Materials Science and Engineering, Tokyo Institute of Technology, Yokohama 227, Japan

‖ Institut de Recherches sur la Catalyse, 69626 Villeurbanne, Lyon, France.

• Abstract published in *Advance ACS Abstracts*, October 15, 1993.

(1) Israelachvili, J. N. In *Intermolecular and Surface Forces*; Academic Press: London, 1985.

(2) Binnig, G.; Quate, C. F.; Gerber, C. *Phys. Rev. Lett.* **1986**, *56*, 930.

(3) Blackman, G. S.; Mate, C. M.; Philpott, M. R. *Phys. Rev. Lett.* **1991**, *65*, 2270.

(4) Joyce, S. A.; Thomas, R. C.; Houston, J. E.; Michalske, T. A.; Crooks, R. M. *Phys. Rev. Lett.* **1992**, *68*, 2790.

(5) See also the review paper by Radmacher, M.; Tillmann, R. W.; Fritz, M.; Gaub, H. E. *Science* **1992**, *257*, 1900, and references therein.

(6) Salmeron, M.; Folch, A.; Neubauer, G.; Tomitori, M.; Ogletree, D. F.; Kolbe, W. *Langmuir* **1992**, *8*, 2832.

(7) Whitesides, G. M.; Laibinis, P. E. *Langmuir* **1990**, *6*, 87.

(8) Strong, L.; Whitesides, G. M. *Langmuir* **1988**, *4*, 546.

(9) Chidsey, C. E. D.; Liu, G.-Y.; Rowntree, P.; Scoles, G. *J. Chem. Phys.* **1989**, *91*, 4421.

(10) Kim, Y.-T.; Bard, A. J. *Langmuir* **1992**, *8*, 1096.

(11) Porter, M. D.; Bright, T. B.; Allara, D. L.; Chidsey, C. E. D. *J. Am. Chem. Soc.* **1987**, *109*, 3559.

(12) Radmacher, M.; Tillman, R. W.; Fritz, M.; Gaub, H. E. *Science* **1992**, *257*, 1900.

0743-7463/93/2409-3600$04.00/0

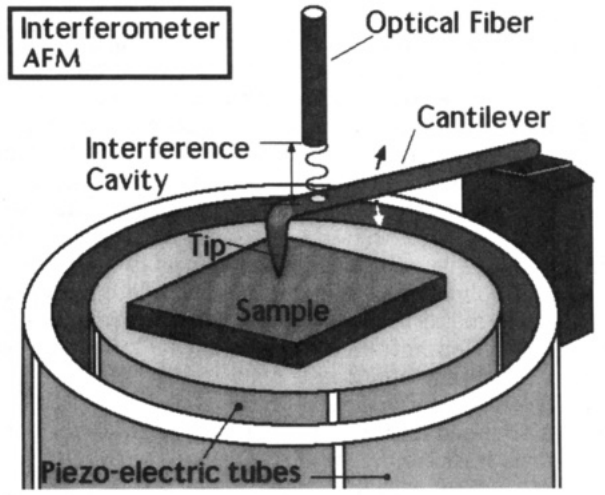

Figure 1. The schematic diagram of the interferometer AFM used in this work. Two concentric piezoelectric tubes support the sample (inner tube) and the tip (outer tube). A smaller piezo slab is used to oscillate the cantilever. An optical fiber is positioned a few micrometers from the back of the tip. Interference between light reflected at the fiber–air and wire–air interfaces provides the lever deflection measurement.

displacement of the cantilever tip, as shown in the schematic drawing of Figure 1. The head consists of two piezoelectric tubes of 0.85- and 0.50-in. o.d.'s and 1-in. length mounted concentrically. The cantilever is attached to the edge of the outer tube by magnetic clamping. A small piezoelectric slab attached to the magnet can oscillate the cantilever for ac measurements. The sample is mounted on a holder supported by the inner piezo tube.

The tips used in the experiments were prepared from 75 and 127 μm diameter Pt–Rh (13%) alloy wires. Their length was typically 2–4 mm and they were bent in an L shape. The end of the short arm of the L was etched electrochemically in a molten salt solution of 80% $NaNO_3$ and 20% NaCl. By application of a bias of +2 V, the tip was sharpened to a radius of around 0.1 μm, as determined by scanning electron microscopy. The mechanical resonance frequency of these cantilevers f_o, varied between 4 and 7 kHz. The Q factor was typically 20–50 and the spring constant k varied between 120 and 320 N/m. The typical noise level in the lever deflection measurements was a few tenths of an angstrom in the bandwidth from 100 Hz to 10 kHz, which translates into a force noise of around 5×10^{-9} N. At low frequency (below 10 Hz), the noise level was several angstroms.

2.2. Modes of Operation. Two basic types of experiments were performed. In the first type, a physical parameter P (P = lever deflection x, oscillation amplitude A, tunneling current I) is measured as a function of sample displacement distance toward the tip, d. This distance is measured from the initial position of the sample, typically a few 100 Å away from the tip. The plots of P versus d are referred to as approach curves (APC's). Any two of these parameters could be measured simultaneously in one APC. The data acquisition time for a typical APC was 0.1 s. In our experiments two curves are always obtained that correspond to the approach and retract parts of the sample displacement. We represent these two curves on the same plot with continuous and dashed lines, respectively. These curves are usually noncoincident. The observed hysteresis is due to a combination of instrumental factors (thermal drift, piezo hysteresis, and creep) and physical effects (adhesion, plastic deformation, etc.).

The lever deflection x is proportional to the force exerted by the tip on the sample. This force F is obtained from x by multiplication by the spring constant: $F = kx$. The displacement d must not be confused with the tip-to-sample separation z. The separation z can be obtained from d and x by substraction: $z = d - d_0 - x$. The distance d_0 is defined by the interaction of the extrapolated asymptotic line from the repulsive part of the force curve and the x axis. This method of obtaining z, however, is only valid for infinitely rigid materials. For real materials, d_0 represents the position of the surface after deformation by the applied force and is different from the position before the application of the load. For this reason we prefer to display the APC data as a function of d, which is measured directly.

In the second type of experiment, the surface is imaged under feedback control. The control parameter was the tunnel current I, in the STM mode, or the cantilever *in-phase* amplitude A, in the AFM ac-mode or attractive mode. In the AFM ac-mode the attractive force gradient above the surface shifts the cantilever resonance frequency and produces a change in A that is very sensitive to the distance. Occassionally the repulsive force measured by the deflection of the tip x was used as the control parameter (dc mode or contact mode AFM imaging). Since our data acquisition software[13] can collect an auxiliary signal in addition to the controlling signal, the following combinations of control and auxiliary parameters were used in different imaging experiments: (1) STM (I = control) + lever deflection (or dc-force). (2) STM (I = control) + amplitude A (or ac-force). (3) ac-AFM (A = control) + current I. (4) dc-AFM (lever deflection x = control).

Because of their special importance we describe the modulation experiments separately. The free resonance frequency of a cantilever is modified by the tip–surface interaction potential, as shown by Dürig et al.[14] This effect can be used to measure and map force gradients on the surface. In our experiments, the cantilever was oscillated by modulating the voltage applied to a thin piezoelectric slab to which the fixed end was attached. The modulated light intensity reflecting back from the tip–fiber cavity, referred to as the lever deflection signal, was measured at the photodetector and fed into a two-channel lock-in amplifier. The phase of the lock-in amplifier was adjusted to maximize the signal in one channel when the lever was far away from the surface. We refer to this as the *in-phase* amplitude A. The quadrature signal B, 90° out of phase with A, was measured simultaneously in the second channel of the lock-in. Near its resonance, as the tip interacts with the surface, the phase and amplitude change. The time constant of the change depends on the ratio Q/f, which in our case is typically 5 ms. Any interaction that changes the force constant of the combined cantilever-surface system, will produce large changes in A and B.[15,16] These two parameters are thus very sensitive to the presence of forces near the surface. Before contact these are due mainly to capillarity and van der Waals interactions. When the tip was in contact with the surface, the main contribution was from the viscoelastic response of the molecular monolayer.

2.4. Sample Preparation. The gold samples were produced by vacuum evaporation onto a mica or silicon wafer substrate.[17] When observed in the STM, the films grown on mica showed large flat terraces and monoatomic steps, characteristic of the (111) orientation. Atomically resolved images showed the hexagonal lattice of Au(111). On silicon, the gold crystallites were smaller but exposed also many flat terraces. Many of these had straight boundaries crossing at 60° and 120° angles that are characteristic of the (111) orientation.

Thiolate monolayers were formed by adsorbing the thiols from dilute ethanol solutions onto the freshly deposited gold films. Characterization of the monolayers was performed by means of ellipsometry, infrared, and contact angle measurements. This is described in detail in the paper by Chidsey and Loiacono.[17] The thiol compounds $H–S–(CH_2)_n–CH_3$ had chain lengths with 12 and 22 carbons. For brevity, we shall refer to the films they formed as C12 and C22 layers.

3. Results

Thiolate monolayers on gold and siloxane monolayers on SiO_2 with chain lengths above 12 carbons self-assemble to form very sturdy layers, mechanically protecting the

(13) Developed by D. F. Ogletree. Licensed to RHK Technology. Rochester Hills, MI 48309.
(14) Dürig, U.; Gimzewski, J. K.; Pohl, D. W. *Phys. Rev. Lett.* **1986**, *57*, 2403.
(15) Marti, O.; Drake, B.; Hansma, P. K. *Appl. Phys. Lett.* **1987**, *51*, 484.
(16) Erlandsson, R.; McClelland, G. M.; Mate, C. M.; Chiang, S. *J. Vac. Sci. Technol.* **1988**, *A6*, 266.
(17) The gold on silicon samples were kindly prepared by C. E. D. Chidsey. AT&T Bell Labs. Murray Hill. The characterization is described in *Langmuir* **1990**, *6*, 682.

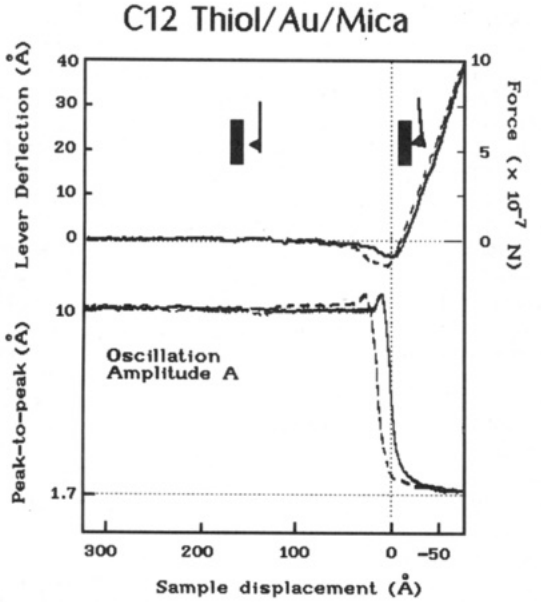

Figure 2. Approach curves showing the lever deflection or force versus sample displacement (top curve) for a monolayer of –S–$(CH_2)_{11}$–CH_3 on a 2000 Å film of Au(111) on mica. Continuous curves correspond to the sample displacement toward the tip while broken line curves correspond to the reverse displacement away from the tip. The bottom curves show the in-phase oscillation amplitude A of the cantilever driven slightly below resonance (4–7 kHz). The origin of the x-axis has been set arbitrarily at the position of the minimum of F in the approach curve.

substrate.[18] In addition, these monolayers electrically insulate the metallic Au substrate, as shown in electrochemical experiments.[19] We have found considerable variation in the monolayer conductivity which, we believe, is due in part to attachment of contaminating material to the metallic tip. The application of forces (compression) can modify molecular conformation locally and produce entanglement of the molecules that give rise to viscous effects. This viscoelastic modification can relax at least partially, in time scales of tenths of seconds, i.e., comparable with experimental times, as shown by Joyce et al.[4] As already discussed in our previous paper on bare gold,[6] the studies of interaction forces between a sharp tip and the substrate conducted in air are plagued with difficulties that are related to (a) contamination effects and (b) poor control of the tip condition. In spite of this, useful information can be obtained that is presented in the following sections.

3.1. Approach Curves. 3.1.1. Force Curves. Figure 2 shows a typical low load APC for a monolayer of C12 on a Au(111) film on mica. In low load experiments, the maximum applied force at the end of the approach curve is less than about 1×10^{-6} N, and the dominant interactions are mainly elastic and reversible, as we shall describe later. The origin of the distance axis has been arbitrarily positioned at the minimum of F in the approach part of the curve (continuous line). The first feature observed as the sample gets close to the tip is an attractive force that becomes measurable at distances of 20–40 Å before the point of zero net force. The depth of the well corresponds to a force F_m^i that varies between 1×10^{-8} and 2×10^{-7} N for different experiments. The variation is most likely due to contamination that produces capillary forces as well as to variations in tip radius. After the minimum of F, the repulsive component of the force dominates and the sample pushes the tip back. The initial curvature is related to the elastic deformation of the contacting bodies.[6,20] After a maximum force or load, F_M, is reached, the sample is retracted, and the broken line curves are obtained. Other examples of force APC's are shown in Figures 3, 4, and 5. If F_M does not exceed about (2–5) $\times 10^{-6}$ N, the attractive force minimum F_m^o found on retraction is usually similar to that found on approach F_m^i. However, for larger loads, F_m^o sometimes was substantially larger than F_m^i, as shown in the example of Figure 5a. This is probably due to formation of strong chemical bonds when the thiolate layers are disrupted and metal–metal contacts form. This behavior is substantially different from the case of bare gold substrates.[6] There, strong metallic bonds form readily upon contact, that is, even when F_M is still in the attractive well. The results obtained for C22's on gold films on mica or silicon substrates were similar to those obtained with the C12's.

3.1.2. Effect of Contaminants. Contaminant layers on the tip or on the surface can produce visible changes in the APC's. Not surprisingly, these changes are variable from one experiment to another. One example is shown in Figure 3a. The retract curve shows a couple of weak steps due probably to mobile material that is attached to the tip and stretches into a neck that breaks at points 2 and 3. Similar effects have been observed by Mate.[21] An even smaller step is seen in the approach curve and is marked by (1) in the figure. Another example of contaminant effects is shown in figure 3b. The force curve (a′) in this experiment shows an initial slope after the minimum that is smaller than normal, due to the compression of interposed material that is softer than the substrate. Sometimes the contaminating material is displaced after one or several approach curves. In the example of Figure 3b, a second approach curve (b′) taken on the same spot immediately after (a few seconds) indicates that some of the contaminants have been displaced. In many cases, the effect of contaminants is very weak and can only be seen easily in the oscillation amplitude curves (to be discussed next) like those shown in the bottom panels of parts a and b of Figure 3. The type of contamination that produces these changes probably consists of mobile material that is weakly bound. Often however, the only signature that can be observed is a slow decrease of A around the minimum of F, like in curve b′ of Figure 3b. We attribute this to more strongly bound contaminants attached to the tip. Contamination also modifies the current APC's as we will see later. We found that pulsing the tip to a few volts is an efficient way to restore the APC curves to their "normal" appearance (like in Figures 2, 4, and 5). It is for this reason that we think the tip is the primary region of attachment of the more strongly bound contaminant material.

3.1.3. Oscillation Amplitude Curves. Examples of the APC corresponding to the *in-phase* oscillation amplitude A are shown in the bottom or middle panels of Figures 2, 3, 4, and 5 for both the C12 and the C22 thiolates. Figure 4b shows an example of A together with the *quadrature* component B. The amplitude A has the following general characteristics in all the APC's: It starts with a set value A_0 of around 10 Å peak-to-peak at large separations. A few 10's of angstroms before the minimum of F, when the attractive force becomes measurable, A increases. It reaches its maximum value a few angstroms before the minimum of F, and then decays rapidly. The extent of the increase in A depends strongly on the initial offset between the driving frequency f and the resonance

(18) DePalma, V.; Tillman, N. *Langmuir* **1989**, *5*, 868.
(19) Finklea, H. O.; Avery, S.; Lynch, M. *Langmuir* **1987**, *3*, 409.
(20) Cohen, S. R.; Neubauer, G.; McClelland, G. M. *J. Vac. Sci. Technol.* **1990**, *A8*, 3449.
(21) Mate, C. M. *Phys. Rev. Lett.* **1992**, *68*, 3323.

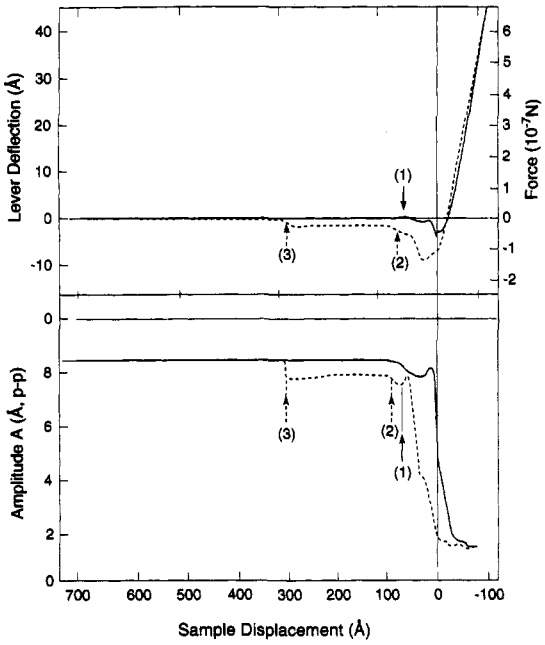

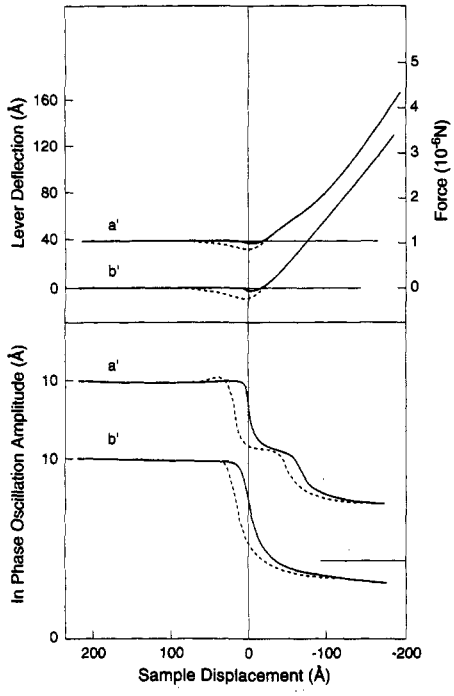

Figure 3. Effects of contaminant layers are shown in these two examples: (a, top) Approach curves showing the force (top panel) and in-phase oscillation amplitude A (bottom panel) for a $-S-(CH_2)_{11}-CH_3$ monolayer on Au on mica. Contamination layers give rise to the steps visible in the force curves due to formation of capillarity contacts (point 1) and the breaking of bridge necks developed upon retraction (points 2 and 3). The corresponding changes in the A curves are shown below. (b, bottom) Approach curves showing other types of contaminant effects. Curves a' correspond to a contaminant layer that can be compressed (initial lower slope in F) and removed after several successive approach curves (b'). The oscillation amplitude curves permit detection of the presence of contaminants more easily (bottom panel).

frequency of the free lever f_0, decreasing to zero when f approaches f_0. At the minimum of F, A has decreased to approximately 50% of its original value A_0. Unlike the case of clean gold studied previously,[6] A does not decrease to zero past the minimum of F. Instead, it remains at a value of about 15 ± 4% of A_0 for the C12 and 18 ± 4% for the C22 films. Finally, when the load reaches values of about (0.7 to 1.5) × 10^{-5} N, it decreases to zero. Figure 4 shows an example of a C12 monolayer on gold on mica

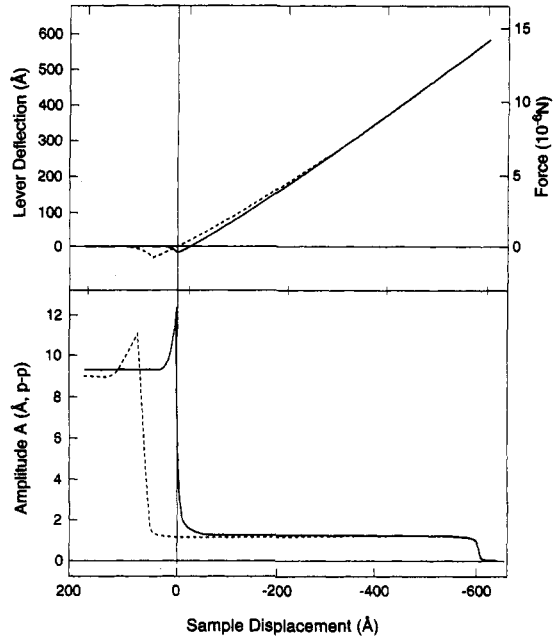

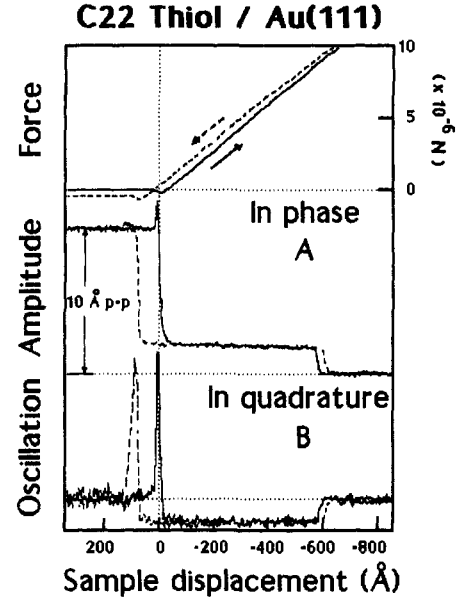

Figure 4. (a, top) Approach curves for a $-S-(CH_2)_{11}-CH_3$ monolayer on gold on mica with a maximum force of 1.5 × 10^{-5} N. Notice the curvature of F after the minimum that is due to the deformation of the contacting bodies. The in-phase oscillation amplitude (A) shows a sharp increase due to the attractive forces followed by an equally sharp decay. The amplitude is reduced by about 50% at the minimum of F. A residual oscillation (14%) persists during the compressive regime. The amplitude decreases to zero when the load is about 1.4 × 10^{-5} N. The broken lines show the retract part of the curve. Drift and piezo hysteresis are responsible for the crossing of the two curves. (b, bottom) Force (top), in-phase A (middle) and 90° out-of-phase B (bottom) oscillation amplitudes for a $-S-(CH_2)_{21}-CH_3$ monolayer on gold on silicon. The behavior is very similar to that shown in (a) for the C_{12} monolayer, except for a smaller reduction of A during the compressive regime (18%). The B signal shows a sharp maximum just when A is reduced to 50% and very close to the minimum of F. In the compressive regime it remains approximately constant and negative, indicating a phase change of more than 90°. This indicates a repulsive restoring force.

(a) and a C22 monolayer on gold on silicon (b). The corresponding changes in B during the APC are as follows: B is zero at large distances and increases very rapidly about the same time when A increases. It goes through a sharp maximum past the maximum of A, just when this amplitude has decreased by 50%. After the maximum, B decreases rapidly and becomes negative,

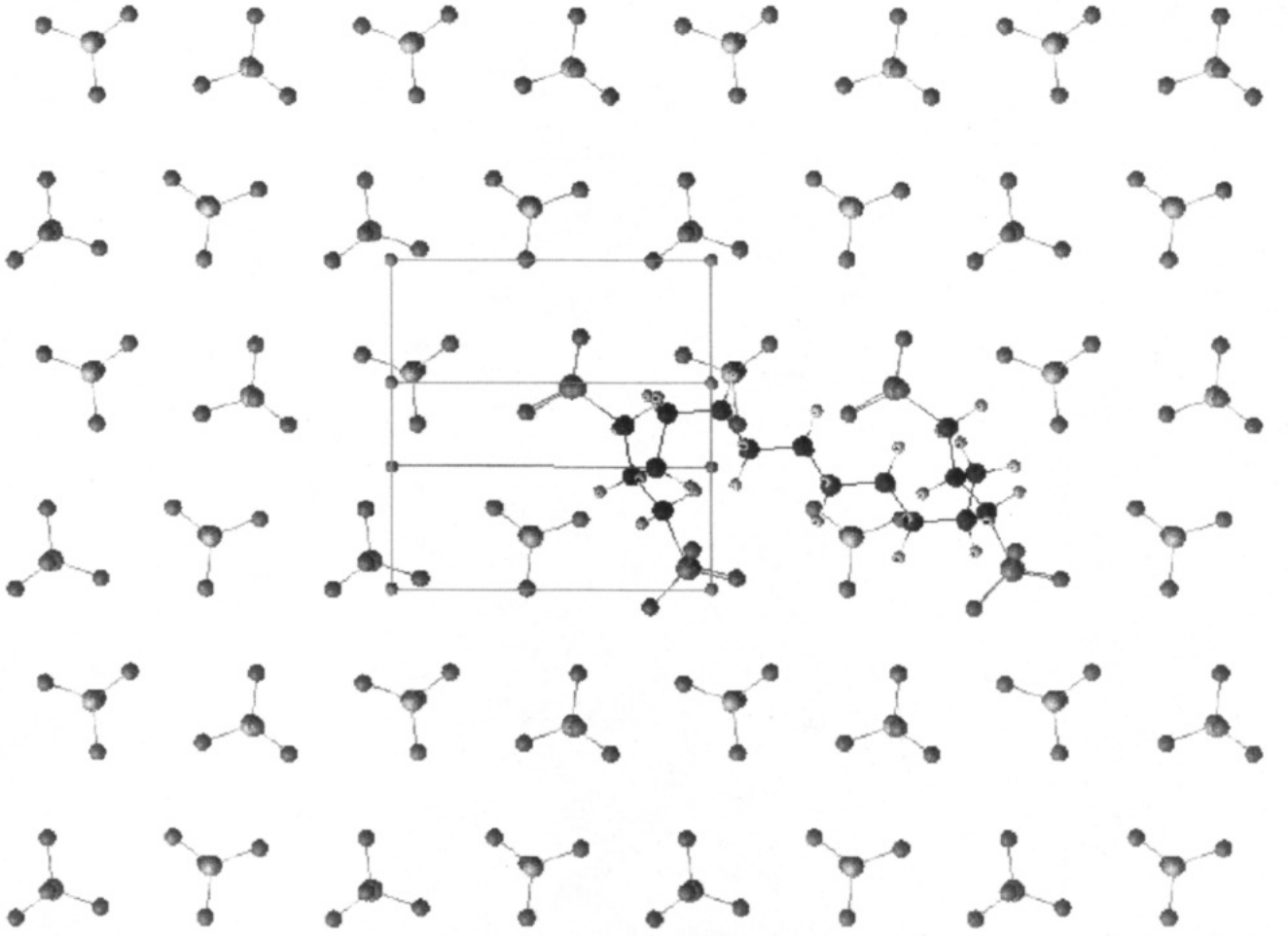

Figure 3. Representation of additive **5** occupying two adjacent binding sites on the (011) surface.

phonate itself—provided that both of the active groups can simultaneously access the same surface.

It was necessary, therefore, to consider how the two active motifs could be linked together and to understand the requirements of this link. Structural analysis of the (011) face revealed that the most efficient design for new molecules was one that allowed the two active groups to access a separation of *ca.* 9.0 Å (Figure 1). Further modeling revealed that links at least 7.4 Å long would allow this. (Here the length of the link is defined as the separation between the two terminal carbon atoms bonded to the two nitrogen atoms of the active groups.) The minimum link length represents the situation where the link would be fully extended for the active groups to access two adjacent sites. A slightly longer link, e.g., 8.5 Å, would allow for some minimization of steric interactions because of the extra flexibility, and so these molecules might be more effective. Figure 3 demonstrates these ideas, for a 10-carbon link, showing how the alkyl chain can adopt a low-energy conformation above the surface, hence enhancing the performance of the additive as a growth inhibitor.

It is conceivable that there is also a maximum link length above which a combination of solubility and conformational factors act to reduce efficacy. This is not easily determined by molecular modeling but could be assessed using experimental data.

The molecules to be synthesized, therefore, had to satisfy the following requirements: (1) the two active groups must be able to access a separation of 9.0 Å and (2) both groups must be able to easily access the same surface simultaneously. These criteria had to be satisfied regardless of whether the intergroup link was rigid or flexible. Molecular modeling was then used to identify suitable candidate molecules. A series of possible intergroup links were constructed, and only those satisfying the above criteria were selected. Then retrosynthetic analysis was performed on the potential additives that contained these intergroup links. Only those compounds with feasible synthetic routes were considered for synthesis; some examples are displayed in Figure 4.

These design criteria relate specifically to binding on the (011) face. As noted earlier, however, these molecules are also likely to influence the (210) face. The separation between adjacent binding sites on this surface is *ca.* 7.1 Å. This suggests that molecules designed to simultaneously access two adjacent sites on the (011) face may also bind to the (210) face in a similar way. It is further evident that the more complex geometry of the sulfate array on the (210) face compared to the (011) face may allow these molecules to access alternative binding sites and hence further enhance their potency.

Experimental Section

Synthesis. The compounds identified by the above work were synthesized from their respective diamines following the Mannich-type reaction reported by Moedritzer and Iran.[8] The general procedure for this reaction was as follows:

$$H_2NRNH_2 + 4H_3PO_3 + 4HCl + 8HCHO \rightarrow (H_2O_3PH_2C)_2NRN(CH_2PO_3H_2)_2$$

R represents a flexible link. A wide variety of chemicals were used. For hydrocarbon chains the starting diamines were

(8) Moedritzer, K.; Irani, R. *J. Org. Chem.* **1966**, *31*, 1603.

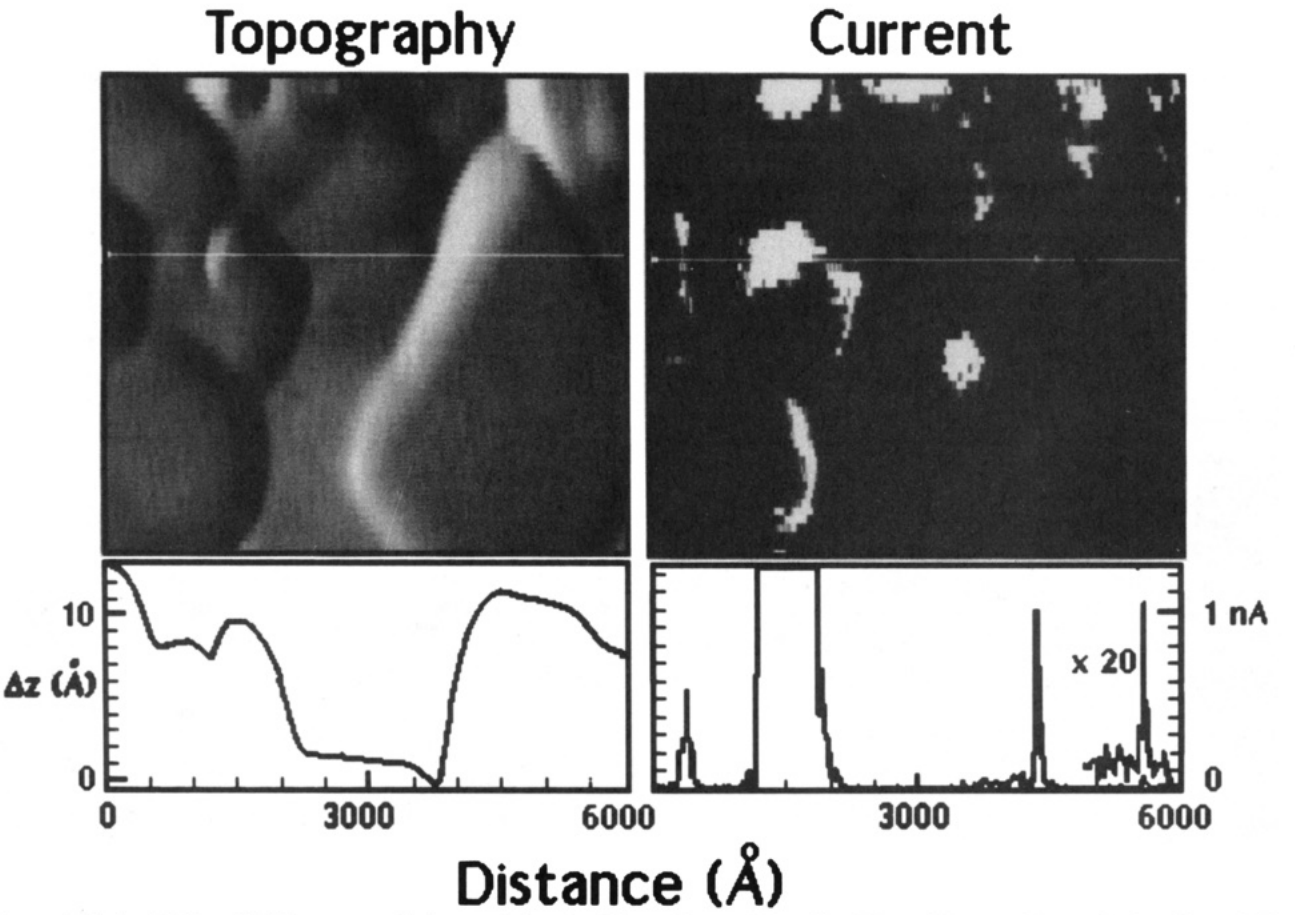

Figure 6. Left: 6000 × 6000 Å topographic image (left) of gold on silicon with a $-S-(CH_2)_{11}-CH_3$ monolayer, displayed as a light-shaded image to enhance contrast. The image is taken in the ac-mode at 50% reduction of amplitude A. Right: Simultaneously acquired current map at a 10-mV bias. High conductivity areas correspond to grain boundaries and defect areas. Cursor profiles across the images are shown at the bottom.

we show an ac-AFM image of a C22 monolayer on gold on mica, taken at a set point corresponding to 20% reduction in A_0. This regions contains steps that are vaguely discernible in the image. Immediately after this we used the current I as control for our feedback at a set point of 10 nA and a bias voltage of 20 mV, which produced the image labeled b in the figure. The image is shifted by about 1000 Å to the left relative to (a) but the same general features can be easily recognized. As we can see the resolution of the STM image is considerably higher than that of the AFM image as shown by the better resolved step structures. This occurs in spite of the fact that according to the APC curves for A and I, the tip–surface distance is similar, within a few angstroms for both imaging modes. Another ac-mode AFM image obtained immediately after the STM image is shown in (c) and indicates a slight blurring of the features, but no major changes are introduced by the STM imaging.

3.4. Plastic Regime: Indentation Experiments. The plastic response of the substrate was studied by applying loads of increasing value and then imaging the surface to assess the production of indentation marks. The size and depth of the marks were measured to determine a value of the microscopic "hardness", by dividing the load F_M by the projected area of the mark. This procedure was also utilized in the case of bare gold and is described in our previous paper.[6] The values obtained are 0.6 ± 0.3 GPa, very similar to those obtained on bare gold. This indicates that the presence of the thiolate monolayers does not modify the plastic behavior of the gold substrate. Examples of such marks can be seen in Figure 9 for the C12's and in Figure 10 for the C22's. The threshold load for the production of visible marks like those shown in these two images is around 1 to 2 × 10^{-6} N for the ~1000 Å radii of our tips. Interestingly, the amplitudes A and B are still nonzero at these loads (see Figure 4), indicating that the gold substrate yields plastically before complete attenuation of the cantilever oscillation. The current images obtained simultaneously with the ac topographic images allowed us to assess the change of electric properties of the thiolate film around the plastically deformed areas. A region of higher conductivity was always found around the indentation mark as shown in Figures 9 and 10. The center of this region, corresponding to the bottom of the hole, exhibits very low conductivity, like the undistorted areas. It appears then, that even after the application of loads above the plastic limit of gold, the thiolate molecules can relax back to their initial conformation except in the areas where the shear of the Au substrate exposes fresh gold and where numerous steps are probably generated.

4. Discussion

4.1. The Damped Harmonic Oscillator Model. In order to facilitate the discussion of the modulation experiments, we consider the motion of a harmonic oscillator driven by a periodic signal in an external force field. The equations of motion of such a system are described and solved in classical mechanics textbooks. A more detailed account applied to the AFM can be found elsewhere.[22,23] In our experiments, the phase of the lock-in amplifier is set to maximize the output signal A in one channel, far away from the surface. It can be shown that the expression for this signal is

(22) Dürig, U.; Züger, O.; Stalder, A. *J. Appl. Phys.* **1992**, *72*, 1778.
(23) Salmeron, M. *Mater. Res. Soc. Bull.* **1993**, (May).

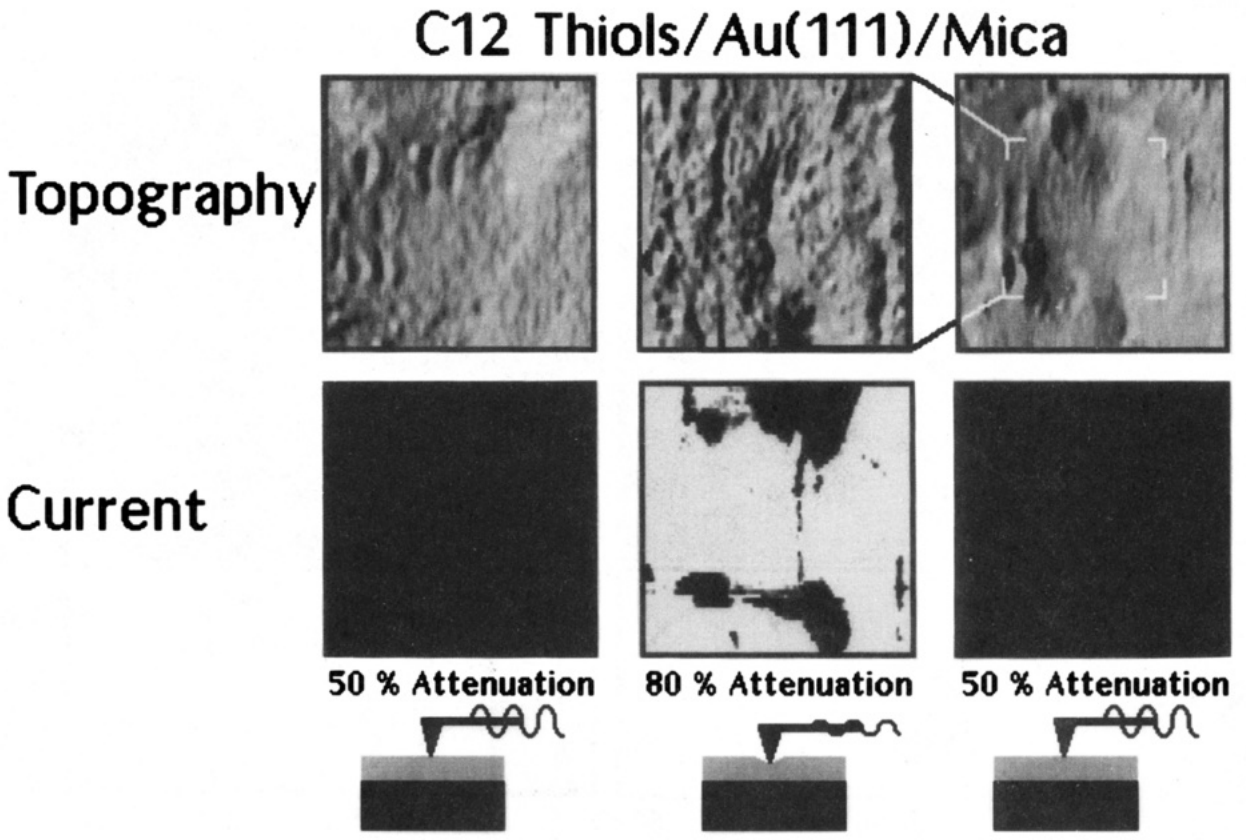

Figure 7. Left: 5000 × 5000 Å AFM topographic image (light shaded) of a gold film on mica with a S–$(CH_2)_{11}$–CH_3 monolayer. Image obtained in the ac-mode at 50% reduction of A. Simultaneously acquired current image is shown at the bottom. The bias voltage was 0.1 V. Middle: Same area imaged at 80% reduction of amplitude A. Notice the large increase in the current intensity to hundreds of nanoamperes in most of the image range (bright areas). Right: 8000 × 8000 Å images at the original 50% reduction of amplitude A. The central 5000 × 5000 Å region shows a shallow depression of 1–3 Å relative to the surrounding area. Material accumulated at the end of the scan lines of two previous images at the higher reduction is visible. The height of these edges is 3–5 Å.

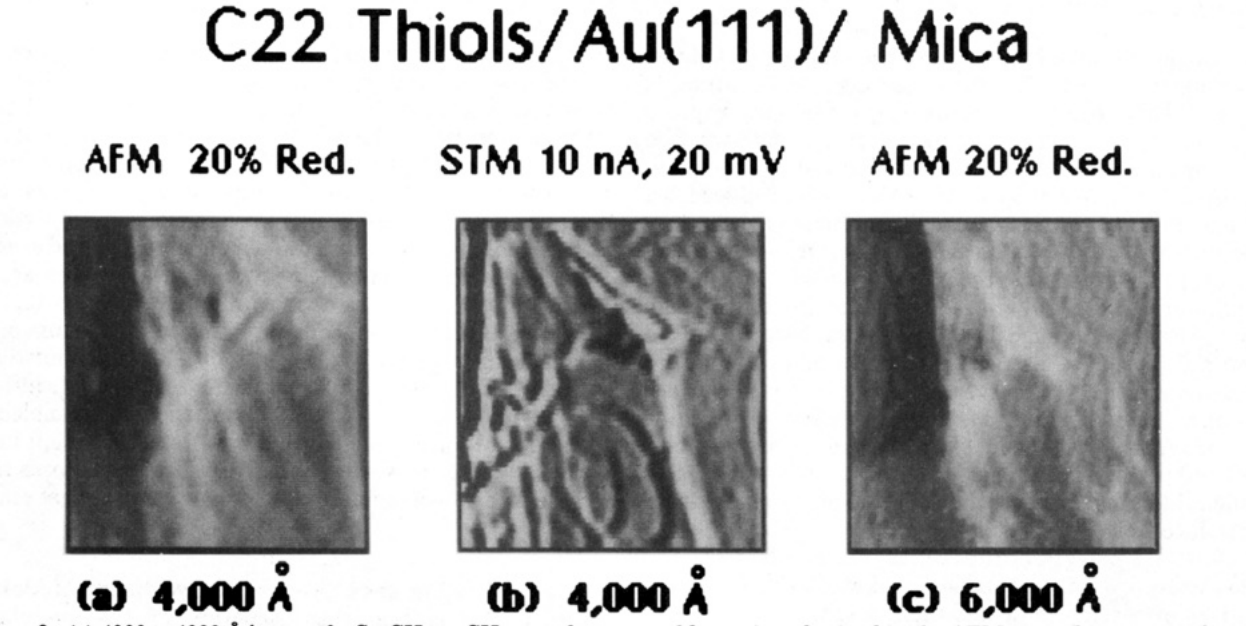

Figure 8. (a) 4000 × 4000 Å image of a S–$(CH_2)_{21}$–CH_3 monolayer on gold on mica, obtained in the AFM ac-mode at 20% reduction of A. (b) 4000 × 4000 Å STM image of the same region (a drift in the upward and right-hand directions occurred during adjustments). Current set point is 10 nA, bias voltage 20 mV. (c) 6000 × 6000 Å ac-AFM image obtained after the STM imaging experiment.

$$A = \frac{aQ}{(1-\delta+\delta^2Q^2)^{1/2}} \frac{1-\delta+\delta\,(\delta-f'(z))Q^2}{1-\delta+(\delta-f'(z))^2Q^2}$$

where a is the amplitude of the externally applied modulation at the attachment point of the cantilever, Q is the quality factor of the system which is determined by the frictional forces acting on the cantilever, and δ is related to the offset of the driving frequency f from the mechanical resonance of the free cantilever f_0 through $\delta = 1 - f^2/f_0^2$. Finally, $f'(z)$ is the derivative of the interaction force between tip and surface in units of the cantilever spring constant k ($=k^{-1}\mathrm{d}F/\mathrm{d}z$). The first factor in the above expression is A_0, the value of A far away from the surface when $f'(\infty) = 0$. Typical values of these parameters in most of our experiments are A_0 = 5–10 Å peak-to-peak, $Q \approx$ 20–30, and $\delta \approx$ 1–5%. The quadrature signal B is

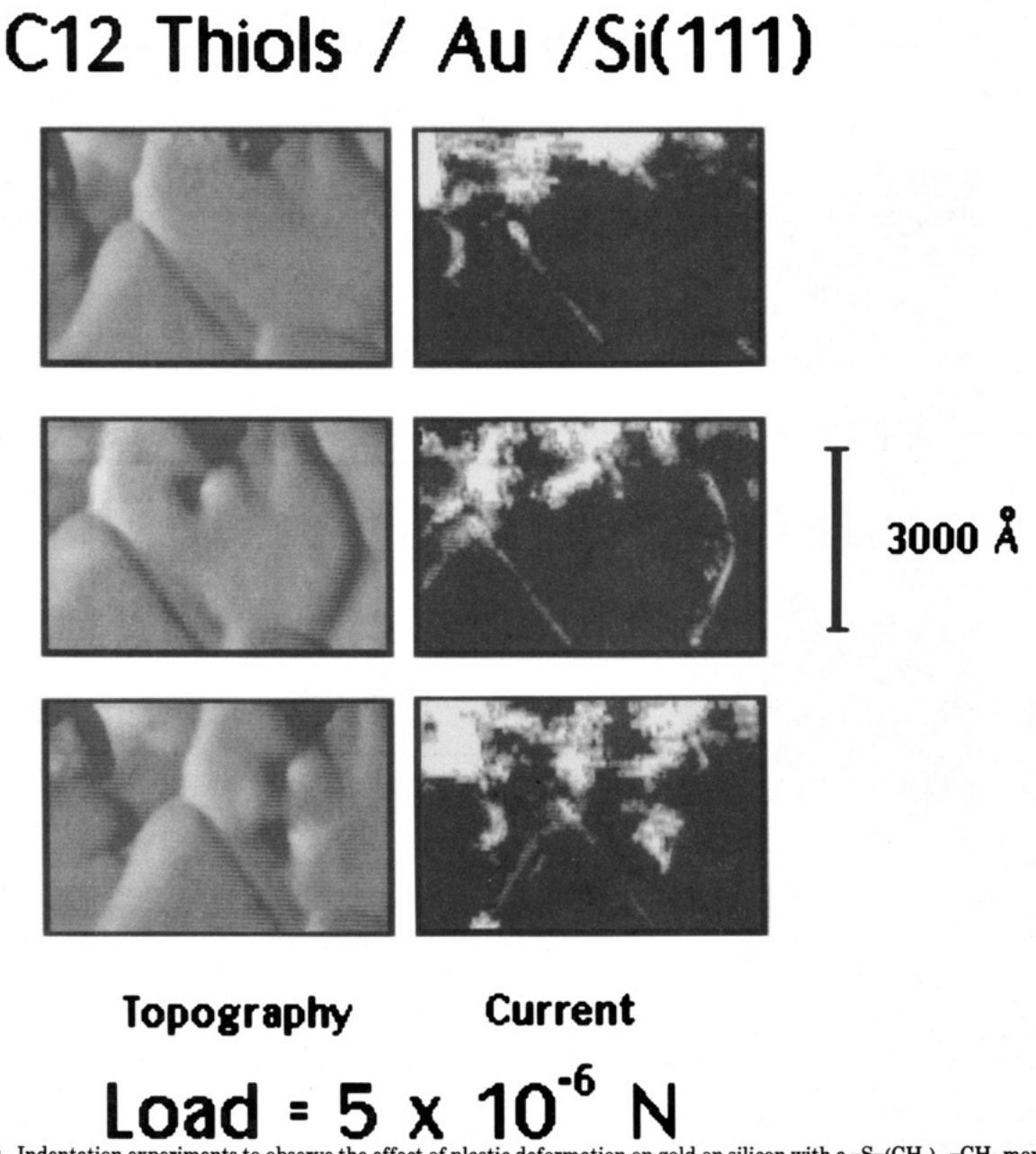

Figure 9. Indentation experiments to observe the effect of plastic deformation on gold on silicon with a $-S-(CH_2)_{11}-CH_3$ monolayer. The 6000 × 4000 Å images are obtained in the ac-mode at 50% reduction of amplitude A and displayed light shaded for better contrast. The surface before indentation is shown on top and after contact (below) at two loads of (5.5 and 4.5) × 10^{-6} N. The two indentation marks have depths of about 70 Å. Current maps at 0.1 V bias show current at the grain boundaries and at defective areas. Additional current is observed around the two indentation marks.

$$B = \frac{aQ}{(1 - \delta + \delta^2Q^2)^{1/2}} \frac{f'(z)Q(1 - \delta)^{1/2}}{1 - \delta + (\delta - f'(z))^2Q^2}$$

The signal B is zero when there is no interaction between the tip and the surface ($f'(\infty) = 0$).

4.1.1. Oscillator in a van der Waals Force Field. In the attractive region, when $f'(z)$ is positive, the amplitude A increases as the tip gets closer to the surface (if $\delta > 0$). This is due to the "softening" of the oscillator in the attractive force field that brings the resonance frequency of the tip–surface system f_0' closer to f. At the maximum $f_0' = f$ and past it, when $f_0' > f$, A decreases rapidly to zero. B varies also from 0 to its maximum value, just when A is equal to $A_0/2$.

In a very simplified model, we shall assume that Q remains constant in the attractive region, before contact with the surface monolayers. The attractive force will be assumed to be of van der Waals origin, i.e. $f'_{attract} = HR/3kz^3$, H being the Hamaker constant (about 4 × 10^{-19} J, from ref 1) and z the separation between tip and surface. The major contribution to $f'_{attract}$ comes from the metallic Au substrate and the tip. The presence of the organic monolayer adds a small term of the form $H'R/3k(z - z_0)^3 - H'R/3kz^3$, where z_0 is the thickness of the monolayer, and H' is the Hamaker constant for the thiolate film (about $^1/_{10}$ that of the metal). With this simple model the experimental A and B vs z curves before contact can be qualitatively reproduced as shown by the curves on the positive side of the x axis of Figure 11 (the origin corresponds to the position of the thiolate surface). Differences in the width of the A and B peaks relative to the experimental ones are related to the modulation amplitude A_0, about 10 Å peak-to-peak, that broadens the experimental peak widths to at least that value. This broadening will eliminate the discontinuity between the attractive part of the curves (left of the origin) and the repulsive part (on the right side) to be discussed below. Another limitation to quantitative comparisons is the

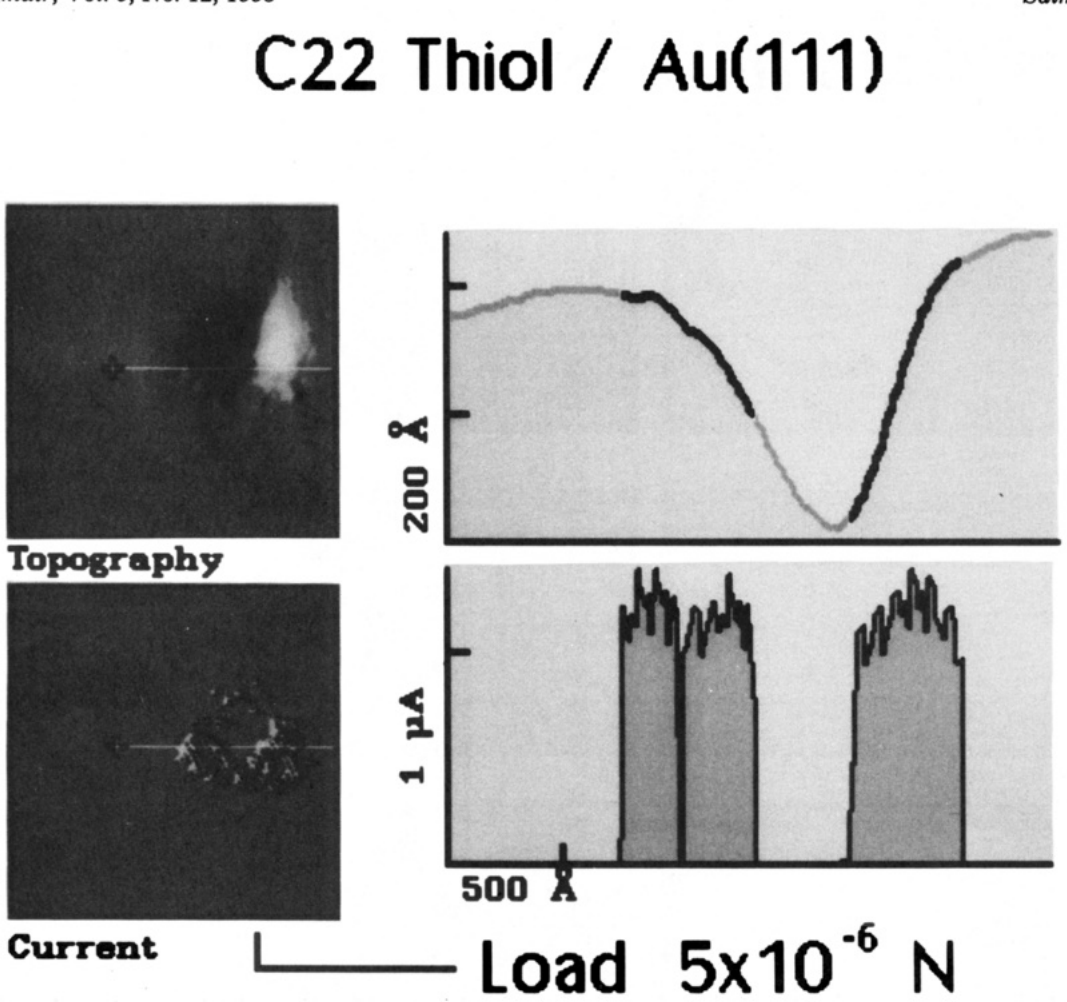

Figure 10. 3000 × 3000 Å topographic and current images (light shaded for better contrast) showing the hole produced after application of a load of 5.6×10^{-6} N. The surface consists of a monolayer of $-S-(CH_2)_{21}-CH_3$ on gold on mica. Current (about 1 μA at 15 mV bias) appears only around the edges or "sides" of the hole, presumably where the numerous gold steps are present due to shear deformation.

assumption of pure van der Waals forces. Other forces including bonding and capillarity forces will act near contact. For these reasons, only the trends in the A and B curves should be regarded as correct.

4.1.2. Oscillator in a Viscoelastic Medium. On clean Au, A and B decrease to zero near the minimum of the force curves, as predicted by the simple model described above, and also because of the formation of metallic contact where the tip becomes effectively "welded" to the substrate, thereby increasing the mass of the oscillator enormously. The presence of the thiolate monolayers modifies this behavior drastically. Instead A decreases to a value that is 10 to 20% of its value at infinite distance and remains nearly constant during sample displacement as the tip is pushed back. When the load increases to about 8×10^{-6} N, the oscillation amplitude decreases to zero. The first decrease to a nonzero value upon initial contact is due to an increase of the resonance frequency of the tip–surface system f_0' ("stiffening") due to the compression and dissipation in the thiolate film. The viscoelastic response of thiolate films to applied tip forces has been observed previously by Joyce et al.[4] These authors estimated a recovery time of the film after application of forces of around 80 ms. The stiffening of the tip–sample oscillator system in this contact regime and the change from attractive to repulsive forces (f' changes from + to −) is responsible for the change of sign of B.

To model the repulsive forces, we assume that the gold substrate deforms as predicted by classical elastic theory. According to the Hertzian sphere-flat configuration, the force is given by[24]

$$F_{Au} = \frac{4}{3}E'R^{1/2}h_2^{3/2}$$

where E' is related to the Young modulus of the Au–Pt tip system. If we use the macroscopic values of the elastic parameters for these metals, $E' \approx 68$ GPa. h_2 represents the deformation of the Au substrate. A schematic diagram describing these parameters is shown in Figure 12. The thiolate molecules are modeled by simple springs, forming an elastic layer with an average spring constant κ per unit area. By writing the equilibrium of forces at the tip–thiolate and thiolate–gold interfaces, we obtain

$$F(z) = kx = \frac{4}{3}E'R^{1/2}h_2^{3/2} = \pi r_0^{\,2}(h_1 - h_2)\kappa$$

where x is the lever deflection, r_0 is the radius of the contact area between tip and the thiolate layer, and h_1 is the deformation depth at the thiolate surface. From these expressions, we obtain the value of f'_{repul} to be used in the expressions for A and B shown above.

During the compression regime there is still a van der Waals attractive interaction with the gold substrate that increases as the thickness of the thiolate layer decreases due to compression. This attraction contributes a positive term f'_{attrac} so that the total $f' = f'_{attrac} + f'_{repul}$. It is the softening of the tip–surface spring due to this term that brings the resonance frequency f_0' back to f_0 and then past

(24) Timoshenko, S. P.; Goodier, J. N. *Theory of Elasticity*; McGraw-Hill Publishing Co.: New York, 1970.

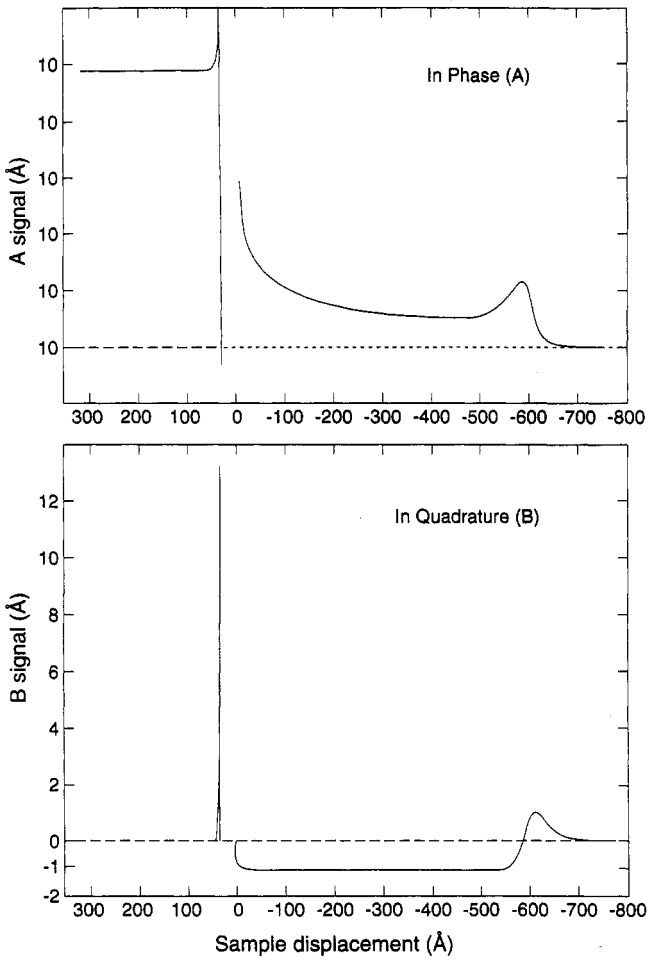

Figure 11. *In-phase* (top) and *in quadrature* (bottom) oscillation amplitude signals for a simple harmonic oscillator driven near resonance in an external force field. The curves at the left of the x-axis origin correspond to the attractive part, before contact. A van der Waals force field was assumed. Tip radius R = 1000 Å; Hamaker constant $H = 4 \times 10^{-19}$ J. Driving frequency offset 10%. The parts of the curves at the right-hand side of the x-axis origin correspond to contact and compression of the organic monolayer. The layer is modeled as a viscoelastic sheet. In this compressive regime, the sample displacement is not the tip–surface separation but includes the deflection of the lever as the tip is pushed by the sample as well as a small contribution from the deformation of the tip, substrate, and thiolate layer.

it, causing both A and B to go to zero. In this simple model, the thiolate layer has been compressed to a thickness of about 3 Å at this point; that is the alkyl chains have been displaced or lie parallel to the surface. By use of the experimental values for δ, A_0, Q, and R (1000 Å) in the above equations, the curves shown in Figure 11 (negative x-axis), were obtained. As can be seen, the model predicts a slower decrease in A than observed experimentally. Also, A does not remain constant, as in the experiments. Other apparent discrepancies are the peaks predicted for A and B before their decay to zero. The most important parameters in the model to obtain a reasonable fit are the elastic constants E' and κ. To obtain values of A and B in the plateau (relative to A_0), comparable to the experimental ones and the right load for the decay of the two amplitudes to zero, the value of the Young modulus E' had to be about 6 times smaller than the bulk value and κ around 5×10^{17} N/m^3. Interestingly, the bulk value of E' can be used to produce the same approximate results in a modified model where a small protrusion of 25 Å radius is added at the apex of the 1000 Å radius tip that indents the gold through the organic layer. Other variations can be introduced in the model that will certainly improve the fit. For example, a stiffening of the thiolate layer as it is compressed might be excepted. The viscosity of the film, that is included in Q, can also change as a function of compression. An example of the prediction of this simple oscillator model is shown in the curves on the right side of the x axis in Figure 11. From the value of κ obtained from the model, a molecular spring constant of 0.1 N/m can be estimated. The characteristic frequency of such a spring for a C22 molecule would be about 2×10^{11} Hz. This value is in the range of soft modes like rotations around the C–C axis (gauche conformations), frustrated translations, and librations consistent with the type of molecular motions leading to a compression of the thiol layer. A "Young modulus" for the thiol film can also be estimated from the elastic constant κ. The value of this modulus is about 2 GPa, which is a factor of 10 higher than the modulus of polyethylene.

There is one underlying assumption in the model that we like to make explicitly here. This is the assumption that the S end of thiolate chain remains attached to its binding site during the compression, so that there is no lateral diffusion of the molecules. The assumption is based on the known chemical and physical properties of thiol and siloxane self-assembled monolayers: compact packing to fill space and the chemical and mechanical inertness of the films.[18,19] In our experiments however, the forces applied by the tip can be very localized in space and produce lateral compression or displacement of the thiol molecules. In this new model, some "vertical" compression could still be occurring, at least during the initial part of the repulsive regime. At some sufficiently high load however, the thiol molecules might be squeezed out of the contact region and compressed into surrounding areas. This load might correspond to the point where A and B fall abruptly to zero, at approximately 1×10^{-5} N. The present data cannot exclude or support this possibility and the assumption needs to be substantiated by further experiments, like those currently in progress in our laboratory.

4.2. Electron Transport through Alkyl Chains. Electron transport through long alkyl chains, and through large nonconducting molecules in general, is an important issue that can be investigated by combined AFM and STM imaging. When the tip contacts the molecular head group, the distance between the metallic tip and the gold surface is equal to the length of the adsorbed thiolate, about 14 Å for the C12's and 25 Å for the C22's. To this should be added the van der Waals radius of the methyl group, about 3 Å. Since alkyl groups are saturated hydrocarbons which are insulating in bulk form, the question arises whether the tip must deform the molecular layer in order to reach the typical tunneling currents used in STM imaging. Electron transport through alkyl chains was investigated by Chidsey et al.[25,26] in electrochemical experiments using ferrocene terminated thiolates. Time constants varying from seconds to milliseconds, depending on the solution–surface potential, were found for the charge or discharge of the ferrocene head group. This provides a clear indication of the poor conductivity of the alkyl chains. When tunneling through vacuum, the tip–metal surface distance is typically about 5 Å,[27] for bias voltages in the range of millivolts to volts and currents of nanoamperes. Higher distances can be achieved by using higher bias voltages and/or lower currents.[28,29] The experimental

(25) Chidsey, C. E. D.; Bertozzi, C. R.; Putvinski, T. M.; Mujsce, A. M. *J. Am. Chem. Soc.* **1990**, *112*, 4301.
(26) Chidsey, C. E. D. *Science* **1991**, *251*, 919.
(27) Gimzewski, J. K.; Möller, R.; Pohl, D. W.; Schlittler, R. R. *Surf. Sci.* **1987**, *189/190*, 15.
(28) Guckenberger, R.; Wiegrabe, W.; Hillebrand, A.; Hartman, T.; Wang, Z.; Baumeister, W. *Ultramicroscopy* **1989**, *31*, 327.

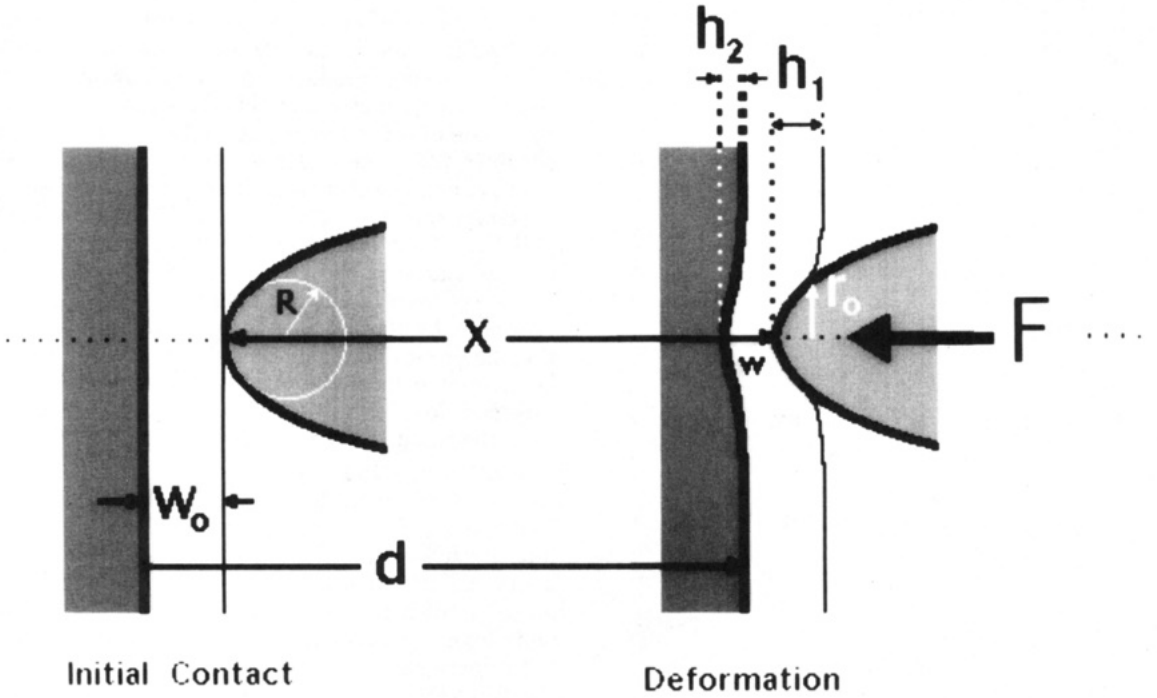

Figure 12. Schematic diagram illustrating the parameters and geometry used to model the compression of the self-assembled monolayers on gold.

results shown in parts a and b of Figure 5 indicate that the current I increases very rapidly at about the minimum of F, where the oscillation amplitude A has decreased sharply to about 50% of its initial value. According to the discussion in the previous section, this corresponds to the initial contact with the methyl end groups of the thiolate molecules.

To understand the mechanism of this electron transport, we performed calculations using the electron scattering quantum chemistry method, that is described in detail in a previous paper.[30] It is based in the use of wavefunction propagators to calculate the electron wavefunction transport from the bulk of one electrode to the other. The tip, tip–methyl gap, and molecular chain are treated as a scattering impurity. In our method, we used the extended Hückel approximation to calculate the matrix elements from the overlap of atomic orbitals. These were s and p orbitals for C and S, and 5d, 6s, and 6p for the gold atoms at the interface. The double zeta asymptotic form was used for the orbitals of the atoms nearest the gap. Both tip and surface are assumed to be gold and the alkanethiolate molecule to be bound through the dehydrogenated S end to an fcc site of Au(111). The result is shown in Figure 13 as a function of tip height for a bias voltage of 50 mV and also as a function of number of C atoms n, in the chain. The kink at the end of each curve signals the contact of the tip with the methyl head group. As we can see in the semilog plot of the figure, all the curves have similar shape and slope, of 1 order of magnitude per angstrom. The variation of the current with chain length, for a given tip distance, is found to increase exponentially with n. This result indicates that the resistance of the chain as a function of length is exponential and not linear. When comparing with the curve for bare gold, we can see that the presence of the alkyl chain greatly increases the tunnel probability by about half an order of magnitude per C atom. This result indicates that the presence of the adsorbed organic molecule enhances the tunneling probability. The calculated value of I upon contact with a C12

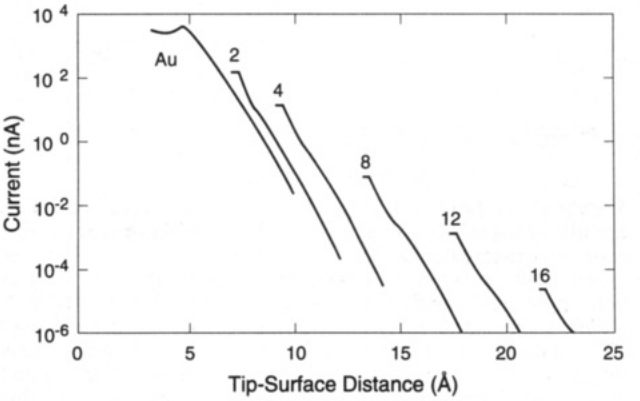

Figure 13. Semilog plot of transmission current between a gold tip and a Au(111) surface with a straight chain $-S-(CH_2)_n-CH_3$ molecule interposed. The current is calculated within the electron scattering quantum chemistry model (see text). The Extended Hückel approximation is used to calculate the matrix elements from atomic orbital overlaps. The bias voltage is 50 mV. Each curve corresponds to a different number of C atoms in the chain, from $n = 2$ to 16. This includes the vacuum gap ($n = 0$, left curve). As we can see, for a given distance the presence of the alkyl chains increases the tunneling probability by about half order of magnitude per C atom.

is approximately 1 pA, and for the C22 the value is immeasurably small. Since our current values increase to much higher values after a few angstroms compression (past the minimum of F), it implies that deformation of the chain by the tip might substantially affect the tunnel conductivity.

We thus investigated the effect of molecular distortions. One important distortion is the bending of the molecular chain axis toward the surface. The result is shown in Figure 14 for $n = 8$. As we can see, the tunneling current increases rapidly above 50°. Our distortion, like rotations about the C–C axis, leading to the formation of gauche defects, was also investigated. The result in that case is similar to that of bending, in the sense that it results in an increase in I when the projected vertical distance to the surface is decreased by the deformation. This agrees qualitatively with our experimental observations although it fails to

(29) Wilson, T.; Murray, M. N.; Ogletree, D. F.; Bednarski, M.; Cantor, C. R.; Salmeron, M. B. *J. Vac. Sci. Technol.* **1991**, *B9*, 1171.
(30) Sautet, P.; Joachim, C. *Phys. Rev. B* **1988**, *38*, 12238.

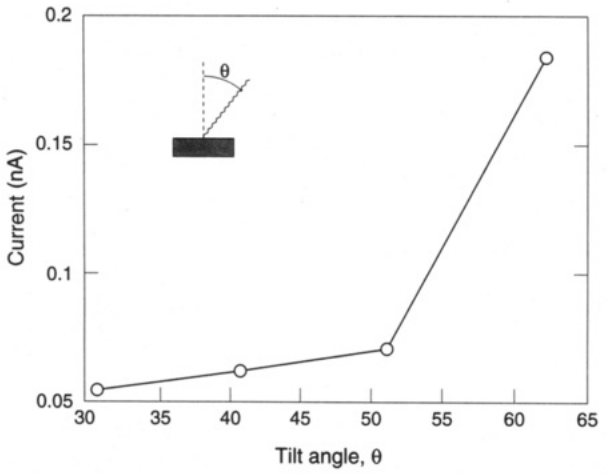

Figure 14. Tunneling current dependence on the inclination of the alkyl molecular axis away from the normal, according to the model calculations as in the previous figure.

predict the magnitude of the increase observed. The discrepancy could be due in part to the fact that in the experiments, many molecules participate simultaneously to the current.

The increase of current observed at grain boundaries and defects can be explained by the lower packing density of molecules at those sites that allow the facile formation of kinks in the chains, driven by thermal excitation and entropic forces. This would result in the tip being closer to the metal surface in these regions.

The enhanced resolution in the STM images like those in Figure 8 deserves a special comment. As pointed out in the Experimental Section, the *I* APC's in parts a and b of Figure 5 indicate that the very rapid increase of *I* occurs at about the same point (within a few angstroms of the minimum of *F*) where *A* decreases. Thus the STM and AFM images are obtained at the same distance from the surface, i.e. the point of contact with the methyl end groups of the thiolate molecules. The observed difference of resolution is qualitatively consistent with the range of the interactions that are sampled in each experiment. The force is contributed by a large area of the substrate since it is due to long range attractive forces and to elastic forces of the monolayer in all the contact area between tip and surface. The tunnel current on the other hand decays exponentially. Therefore only a small protrusion of the tip in the contact area, possibly of atomic dimensions, will contribute all the current. Judging from the step width in Figure 8, about 100 Å, we can conclude that the tunnel current is "channeled" to the surface through at most 400 molecules. The average current per molecule, approximately 25 pA, is still very high in comparison to the value predicted by the calculation. The origin of this enhancement of the tunnel probability is not yet understood at present.

Conclusions

We have shown that the AFM is an important tool to investigate the forces of interaction between sharp tips and surfaces covered with the self-assembled monolayers formed by alkanethiols. Operating the AFM in the ac-mode provides great sensitivity to the interaction forces. Near resonance of the cantilever in particular, the oscillation amplitude decays sharply (within a few angstroms) to a small value when the tip contacts the organic monolayer. This allows imaging, by feedback control of this amplitude, at the thiolate–vacuum interface. At this position, the tip senses a small tunneling current when a bias voltage is applied. This current increases exponentially with decreasing tip–surface distance. In the areas where the thiolate film is not well-packed (boundaries, defects, etc.), the tunnel current during ac-AFM imaging increases to a much larger value.

One finding of our studies is the resistance of the thiolate molecules to external forces. The gold substrate was found to yield plastically, well before the "cushioning" effect of the organic monolayer on the oscillation of the tip ceases. In fact, it appears that after the tilting, bending, and other deformations of the molecules due to the applied load, they relax back to the original conformation after unloading.

Detailed studies of electron transport through large organic molecules that are electrical insulators in the bulk are possible by the combination of STM and AFM techniques. Our theoretical studies indicate that there is a substantial enhancement of tunneling probability by the molecules interposed between tip and surface. This studies indicate also that additional enhancement is obtained by the deformations of the molecules that shorten the average distance between the head group and the surface. Our experimental results are in qualitative agreement with these theoretical predictions.

Note Added in Proof. After submission of this paper, the authors became aware of the recent work by Dürig et al.[31] where a similar AFM-STM study of alkanethiols was performed in UHV. Our findings agree basically with their results, in particular the observation of enhanced tunneling through the alkane chains when the tip is in contact with the monolayer and compresses the molecules.

Acknowledgment. The authors thank C. E. D. Chidsey, presently at the Chemistry Department of Stanford University for preparing the thiolate monolayers on Au films on silicon. This work was supported by the Lawrence Berkeley Laboratory through the Director, Office of Energy Research, Basic Energy Science, Materials Division of the US Department of Energy under Contract Number DE-AC03-76SF00098. Additional support was provided by a grant from Shell Oil Company.

(31) Dürig, U.; Züger, O.; Michel, B. To be published in *Phys. Rev. B.*